Mechanism Model and Prediction Method of Common Mode Radiation for a Nonisolated Very-High-Frequency DC–DC Converter With Cables

Junping He, *Member, IEEE*, Zichao Guo, *Student Member, IEEE*, and Xin Li

***Abstract*—Research on electromagnetic interference of high-frequency power converters remains a challenging and important topic, particularly in light of rapidly emerging wide band-gap power devices operating with ns level turn-ON/turn-OFF times. Building on the substantial contributions that have been made on the formation mechanisms of common mode (CM) radiation, a new mechanism for an equivalent CM driving voltage source caused by imbalanced conductors or components is proposed. Applying this mechanism, the CM driving voltage source model of a nonisolated boost dc/dc power converter with input/output cables is introduced. The CM far-field electric strength algorithms of an asymmetric cable antenna are theoretically analyzed and derived in detail. Subsequently, a prototype for a low-power 30-MHz very-high-frequency boost power converter based on gallium nitride is built and its 10-m CM far-field radiation strength is predicted according to the proposed model. The radiation pattern characteristics are analyzed and several radiation suppression methods are also designed. The comparison with the measured radiation results shows that the proposed CM radiation model and the prediction method achieve good effect below 300 MHz.**

***Index Terms*—Common mode (CM) driving source, equivalent radiation antenna, far-field radiation prediction, generalized common mode potential, very-high-frequency (VHF) power converter.**

I. Introduction

IT IS well known that the electromagnetic radiation emissions (RE) of a power electronic converter can readily exceed the electromagnetic compatibility (EMC) regulations due to their fast switching action. The RE problem remains an important and challenging EMC issue of interest to academia and industry all over the world [1], [2]. With the rapid maturation and application of new generation wide band-gap power devices, such as gallium nitride (GaN) and silicon carbide, faster turn-ON and turn-OFF times, to the ns level, are producing stronger radio frequency spectrums and bringing serious challenges to the EMC designs of modern power converters [3], [4].

The far-field RE of an electrical or electronic device can be decomposed into the common mode (CM) component and the differential mode (DM) component according to the different path properties of the current in conductors [5]. Generally, the DM current in the device generates DM radiation, and this type of current is relatively easy to identify, measure, and predict [6]. In contrast, the CM radiation current is very difficult to identify and predict. The CM radiation current is very small in value (e.g., several or several tens dBμA), and its propagation path and distribution are also very covert and complex. However, the CM radiation does play a very important role below several hundred MHz [7]. In fact, CM radiation is often the main component of the RE for a power converter with cables [8], [9].

Substantial contributions have been made to reveal the formation mechanism of CM radiation and predict the far-field RE [10]–[13]. Watanabe has studied a CM voltage mechanism caused by the radius change of conductors in transmission lines [10]. However, this CM voltage source is derived indirectly, and its physical essence is not clearly explained. Hockanson has proposed equivalent CM sources and an equivalent radiation antenna method for printed circuit boards (PCBs) with attached cables. This method includes a current-driven mechanism and a voltage-driven mechanism [11]. However, the applications of these mechanisms heavily rely on experience and intuition. In addition, accuracy of the mechanism model also needs improvement. He has attempted to apply Hockanson's method to analyze the radiation mechanism and the radiation characteristics of an ac/dc adapter, but its equivalent CM source is just a theoretical model and the error is large [12]. Zhang has proposed a far-field radiation prediction method based on an equivalent CM driving source model, radiated power, and maximum directivity [13]. This method considers the interaction between CM sources and the undesired antenna. Although this method can be used to estimate the radiation strength for an isolated power converter in free space, it is heavily dependent on complex measurements. In addition, the roles of the power switches' current do not receive a detailed analysis in this study.

This article proposes a novel CM driving source analysis method and far-field radiation analytical algorithms to help accurately predict and analyze RE for a power converter.

Manuscript received May 1, 2019; revised August 30, 2019, November 12, 2019, and January 8, 2020; accepted February 12, 2020. Date of publication March 5, 2020; date of current version June 23, 2020. This work was supported by the National Natural Science Foundation of China under Grant 51677035. Recommended for publication by Associate Editor F. Costa. *(Corresponding author: Junping He.)*

The authors are with the Harbin Institute of Technology (Shenzhen), Shenzhen 518055, China (e-mail: hejunping@hit.edu.cn; guozich@126.com; 973688371@qq.com).

Color versions of one or more of the figures in this article are available online at http://ieeexplore.ieee.org.

Digital Object Identifier 10.1109/TPEL.2020.2978278

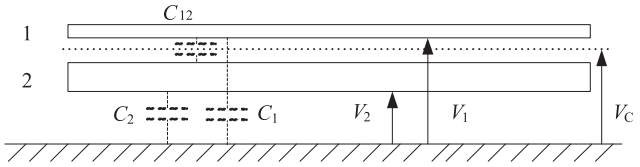

Fig. 1. Two parallel conductors over the ground plane.

To accomplish this, the CM driving mechanism is first discovered and explained based on the concept of a generalized CM potential, which considers the structural imbalance of the conductors and components in system. Then, the CM driving source and the radiation analytical algorithms are implemented and validated using a nonisolated boost dc/dc converter as an example.

The structure of this article is as follows. In Section II, the new generation mechanism and analysis of a CM driving voltage source is introduced in detail. In Section III, the structure of a typical boost converter is introduced. Then, the equivalent radiation model of the converter is deduced and constructed according to the new CM driving mechanism. Subsequently, the analytical algorithms of the far-field radiation of this converter with cables are introduced. In Section IV, the radiation prediction results of a 30 MHz very-high-frequency (VHF) boost converter based on GaN are compared and analyzed by using a 10-m semi-anechoic chamber measurement. The radiation pattern characteristics and several restraining methods are also introduced and analyzed. Finally, the conclusion is summarized in Section V.

II. Generation Mechanism of Common Mode Driving Voltage Source and Radiation

A. Generalized Common Mode Potential Definition

For convenience, the definition of a generalized CM potential is illustrated by a pair of parallel lines in the example below. Fig. 1 shows these parallel lines. The radius of each conductor is arbitrary. Let V_1 and V_2 be the potential of conductors 1 and 2 to the ground plane or infinity, respectively; Q_1 and Q_2 be the charge on conductors 1 and 2, respectively; C_1 and C_2 be the self-capacitance of the conductor 1 and the conductor 2, respectively. The mutual capacitance between the two conductors is set as C_{12}. All these parasitic capacitors are drawn with dotted lines. Then, the charge on each conductor can be expressed as follows:

$$Q_1 = C_1 V_1 + C_{12}\left(V_1 - V_2\right) \tag{1}$$

$$Q_2 = C_2 V_2 + C_{12}\left(V_2 - V_1\right). \tag{2}$$

The sum of the charges T_{total} on the two conductors is as follows:

$$Q_{\text{total}} = Q_1 + Q_2 = C_1 V_1 + C_2 V_2. \tag{3}$$

Let V_C be the CM potential to ground of these two conductors, then their total capacitance T_{total} is the parallel connection of the self-capacitor of each conductor to the ground. This can be expressed as follows:

$$C_{\text{total}} = C_1 + C_2. \tag{4}$$

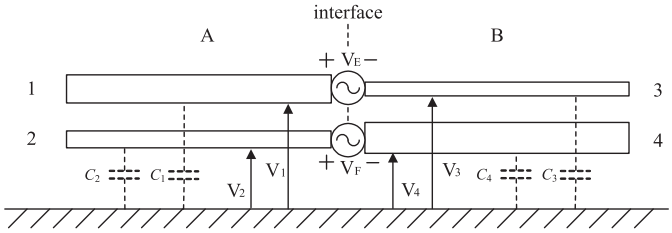

Fig. 2. Connection structure of two transmission lines.

The total charge T_{total} can also be obtained using the following equation:

$$Q_{\text{total}} = \left(C_1 + C_2\right) V_C. \tag{5}$$

Then, the CM potential V_C can be derived as follows:

$$V_C = \frac{C_1}{C_1 + C_2} V_1 + \frac{C_2}{C_1 + C_2} V_2. \tag{6}$$

Here, a coefficient k, the CM potential contribution factor (CMPCF) of a conductor, is defined as follows:

$$k_1 = \frac{C_1}{C_1 + C_2} \tag{7}$$

$$k_2 = \frac{C_2}{C_1 + C_2}. \tag{8}$$

Then, V_C can be rewritten as follows:

$$V_C = k_1 V_1 + k_2 V_2. \tag{9}$$

Obviously, $k_1 + k_2 = 1$. If these two conductors have the same geometry, then $k_1 = k_2$ and V_C is $(V_1 + V_2)/2$, which is the same as the traditional CM potential definition. If these conductors have different geometries, then k_1 and k_2 are not equal. For example, if conductor 2 is a coaxial shielding layer (or an infinite conductor plane), then k_2 is close to 1, and conductor 2 is the main determinant of the CM potential.

B. Generation Mechanism of CM Driving Voltage Source

A typical layout of connecting two transmission lines is shown in Fig. 2. In this figure, the voltage source V_E at the interface represents the voltage of the component (active or passive) that is inserted between conductors 1 and 3. Similarly, the voltage source V_F at the interface represents the voltage of the component (active or passive) that is inserted between conductors 2 and 4. The size of these components is ignored here for idealization. If conductors 1 and 3 are directly connected, then V_E is zero. Similarly, if conductors 2 and 4 are directly connected, then V_F is zero. A CM driving voltage can be generated at the interface position and its formation principle is introduced below.

Let C_1, C_2, C_3, and C_4 be the self-capacitance of conductor 1, 2, 3, and 4, respectively; let V_1, V_2, V_3, and V_4 be the potential of conductor 1, 2, 3, and 4 to the ground plane, respectively; let V_{CA} and V_{CB} be the CM potential to ground of the transmission lines A and B, respectively. Then

$$V_{CA} = \frac{C_1}{C_1 + C_2} V_1 + \frac{C_2}{C_1 + C_2} V_2 = k_1 V_1 + k_2 V_2 \tag{10}$$

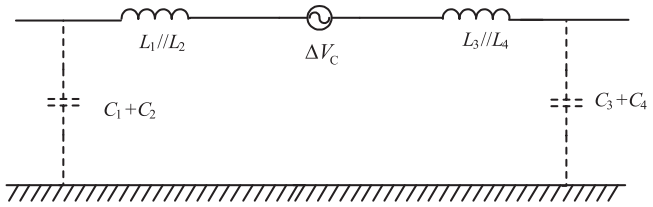

Fig. 3. Formation principle of a CM driving voltage source.

$$V_{CB} = \frac{C_3}{C_3 + C_4} V_3 + \frac{C_4}{C_3 + C_4} V_4 = k_3 V_3 + k_4 V_4. \quad (11)$$

Since there is no fixed relationship among the above parameters, there may be a CM potential difference generated at the interface between transmission lines A and B according to Kirchhoff's voltage law. This is defined as follows:

$$\Delta V_C = V_{CA} - V_{CB} = k_1 V_1 + k_2 V_2 - k_3 V_3 - k_4 V_4. \quad (12)$$

The CM potential difference, $\Delta V_{\rm C}$, can generate the CM current between transmission line A and B, which is shown in Fig. 3. Furthermore, if these conductors are left high enough above ground, the $\Delta V_{\rm C}$ becomes the only CM driving voltage source, transmission lines A and B become radiators. Under these conditions, a new CM RE occurs.

In order to simplify the analysis and deepen the physical insight, two typical cases are illustrated below.

1) CM Driving Voltage Source Produced by Components: In this case, set $k_1 = k_3$, i.e., the structure of transmission line A is the same as or proportional to the structure of transmission line B in cross section, and V_E and V_F are not zero. For $V_1 = V_E + V_3$, $V_2 = V_F + V_4$, the CM driving voltage $\Delta V_{\rm C}$ can be derived from (12) as follows:

$$\Delta V_C = k_1 V_E + (1 - k_1) V_F = k_1 (V_E - V_F) + V_F. \quad (13)$$

As a simple example, if conductor 2 is connected with conductor 4 directly, then $\Delta V_C = k_1 V_E$. This means that a certain proportion of the voltage on the top active or passive component changes into a CM driving voltage source when the transmission line A structure is the same as or proportional to the structure of transmission line B. Similarly, the voltage on the lower component element will become the CM driving voltage source, $(1 - k_1)V_F$ when conductor 1 is directly connected with conductor 3.

2) CM Driving Voltage Source Produced by Structure Change: In this case, let $V_E = V_F = 0$, i.e., $V_1 = V_3$, and $V_2 = V_4$. In addition, k_1 does not equal k_3, i.e., k_2 does not equal k_4. This means that the transmission line A structure is not proportional to the transmission line B structure in cross section. Then, the CM driving voltage, $\Delta V_{\rm C}$, can be derived from (12) as follows:

$$\Delta V_C = (k_1 - k_3)(V_1 - V_2) = (k_1 - k_3) V_{12}. \quad (14)$$

This means that a CM driving voltage source is generated from the DM voltage at the interface, which is consistent with the results in [10].

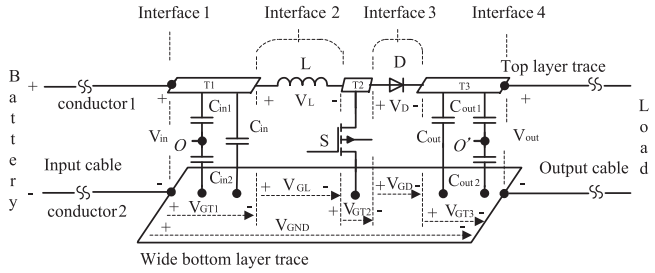

Fig. 4. Main structure of the boost converter.

Incidentally, it is worth noting that $\Delta V_{\rm C}$ is independent of reference potential selection once it is established, which makes it easy to apply.

III. Boost Converter and Its CM Radiation Model

Both an accurate equivalent radiation excitation source model and a reliable unintentional radiation antenna model are the key to obtain effective far-field radiation prediction of a power electronic converter. This section takes a boost converter with cables as a typical example for its radiation modeling and prediction.

A. Boost Converter and Its Structure

The main structures of the boost converter studied are shown by the solid lines in Fig. 4. The main circuit of the boost consists of power semiconductor switches, inductor, capacitors, and PCB interconnections, etc. In particular, the input capacitor $C_{\rm in1}$ and $C_{\rm in2,}$ which are in series and have the same value, are added to input capacitor $C_{\rm in}$ in parallel. The output capacitors $C_{\rm out1}$ and $C_{\rm out2}$ are also in series and have the same value. The voltages across the components or between the nodes are also shown in the figure. For the sake of simplicity, the main circuit layout of the converter is quite regular: the inductor, capacitors, switching devices, and PCB conductors are arranged and installed along a straight line as shown. All of the PCB traces at the top layer, such as T_1, T_2, and T_3, have the same width. The PCB trace at the bottom layer, which serves as a signal ground conductor of the main circuit, is also rectangular and has a wider width. In this figure, only parts of the input/output lines are shown; the load resistor and supply battery are not shown to save space. The input and output cable conductors have the same radius similar to a normal power cord.

B. Equivalent CM Driving Voltage Source Model

Because of the generally regular structure of the above boost converter, its main electromagnetic wave mode can be considered as quasi-transverse electromagnetic wave (TEM). According to the CM driving voltage source mechanism presented in Section II-B, the equivalent radiation excitation source model of the boost converter can be deduced below.

There are four interfaces in the converter, which are shown as Interface 1–Interface 4 by thin dotted lines in Fig. 4. Naturally, four CM driving voltage sources are generated in the model. A PCB trace at the top layer and the signal ground trace just below it form a transmission line. Since all of the PCB transmission

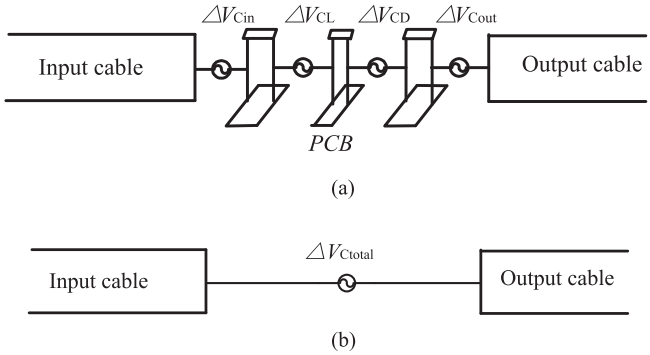

Fig. 5. CM driving voltage sources model of the Boost converter. (a) Four CM driving voltage sources. (b) Simplified CM driving voltage source model.

lines have the same cross-sectional structure in this converter, the CMPCF $k_{\rm trace}$ of these top-layer PCB traces are the same.

Interface 1 is the interface between the input cable and the input port of the PCB. It is clear that the k of the input cable conductors is 0.5, as they have the same radius. So, a CM driving voltage source $\Delta V_{C\rm in}$ is generated according to (14) and is as follows:

$$\Delta V_{C\rm in} = \left(\frac{1}{2} - k_{\rm trace}\right) V_{\rm in}. \tag{15}$$

Interface 2 is the interface formed by the inductor L. As the two PCB transmission lines at both ends of the inductor have the same cross section, so a CM driving voltage source ΔV_{CL} is generated according to (13) and is as follows:

$$\Delta V_{CL} = k_{\rm trace}(V_L - V_{GL}) + V_{GL} \tag{16}$$

where V_{GL} is the voltage drop of the bottom PCB trace just under the inductor L.

Similarly, Interface 3 is the interface formed by the diode D. A CM driving voltage source ΔV_{CD} is also generated and it is as follows:

$$\Delta V_{CD} = k_{\rm trace}(V_D - V_{GD}) + V_{GD} \tag{17}$$

where V_{GD} is the voltage drop of the bottom PCB trace just under the diode D.

At Interface 4, the output port of the boost converter, a CM driving voltage source $\Delta V_{C\rm out}$ is also generated according to (14) and is as follows:

$$\Delta V_{C\rm out} = \left(k_{\rm trace} - \frac{1}{2}\right) V_{\rm out}. \tag{18}$$

After deriving the CM driving voltage sources for the four interfaces, the equivalent CM driving voltage model of the boost converter can be determined. This is shown in Fig. 5(a).

Considering the convenience of application and highlighting the key physical essence, above CM driving sources can be further simplified. Because the size of the boost converter is generally far less than the length of cables and the waveform length of the highest frequency concerned, the radiator effect of the PCB traces of the converter can be ignored. The total CM driving voltage $\Delta V_{C\rm total}$ can be computed by adding the four CM sources together, as defined in (19). This is shown in Fig. 5(b)

$$\Delta V_{C\rm total} = \frac{1}{2}V_{\rm in} + k_{\rm trace}\left(V_L + V_D + V_{\rm out} - V_{\rm in} - V_{GL} - V_{GD}\right) + V_{GL} + V_{GD} - \frac{1}{2}V_{\rm out}. \tag{19}$$

Here, the main electromagnetic wave between the PCB layers is in the quasi-TEM. Consequently, the top layer PCB trace and the signal ground trace just under it conform to the transmission line theory. It can be inferred that the inductance $L_{\rm trace}$ of the top layer trace and $L_{\rm GND}$ of the bottom-layer trace is inversely proportional to the self-capacitance $C_{\rm trace}$ and $C_{\rm GND}$, respectively [14]. So, the CMPCF $k_{\rm trace}$ can be rewritten as (20). In this form, it is easy to see that the middle term in (19), $k_{\rm trace} \times (V_L + V_D + V_{\rm out} - V_{\rm in} - V_{GL} - V_{GD})$, represents the voltage drops along signal ground traces, i.e., $V_{GT1} + V_{GT2} + V_{GT3}$, as shown in Fig. 4

$$k_{\rm trace} = \frac{C_{\rm trace}}{C_{\rm trace} + C_{\rm GND}} = \frac{L_{\rm GND}}{L_{\rm trace} + L_{\rm GND}} \tag{20}$$

Subsequently, the total CM driving voltage $\Delta V_{C\rm total}$ can be simplified as (21). It is clear that $V_{GT1} + V_{GT2} + V_{GT3} + V_{GL} + V_{GD}$ represents the voltage drop across the bottom layer ground trace from the left side to the right side, i.e., $V_{\rm GND}$, which is shown in the bottom of Fig. 4. So, (21) can be further simplified as (22). A careful observation of the formula reveals that $\Delta V_{C\rm total}$ is actually the voltage between the O point and the O' point, which is the middle point of the input capacitors and output capacitors, respectively. This characteristic of the $V_{oo'}$ makes the measurement of CM driving voltage source very convenient

$$\Delta V_{C\rm total} = \frac{1}{2}V_{\rm in} + V_{GT1} + V_{GT2} + V_{GT3} + V_{GL} + V_{GD} - \frac{1}{2}V_{\rm out} \tag{21}$$

$$\Delta V_{G\rm total} = \frac{1}{2}V_{\rm in} + V_{GND} - \frac{1}{2}V_{\rm out} = V_{oo'}. \tag{22}$$

C. CM Radiator Model and Far-Field Prediction Algorithms

The input/output cables, load, and battery of the boost converter constitute a parasitic CM radiation antenna of this power supply system. Since the theory of electromagnetic analysis and the calculation of an unintentional antenna is complex, it is quite difficult and time-consuming to model the parasitic antenna both comprehensively and accurately. Therefore, despite some errors, the battery and the load are treated as a part of the input/output cable to simplify the processing in this study.

The input/output cables of this power converter usually have different lengths and conductor radii, so they actually constitute an electric dipole antenna with different radiation arms. The asymmetric dipole antenna theory is adopted to model and calculate the radiator of the cables in this article. Fig. 6 shows the asymmetric dipole antenna model of the boost power converter system, which can be derived easily from Fig. 5(b). In this model, the input cable and the output cable of the boost converter are equivalent to two long circular conductors. In Fig. 6, the symbol

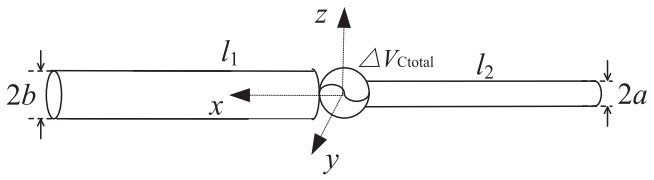

Fig. 6. Equivalent asymmetrical dipole antenna for the boost with cables.

l represents the length of the input/output cable. The symbols a and b represent the equivalent radius r_e of the parallel wires with two cores, which can be calculated according to the following equation [15]:

$$\ln(r_e) \cong \frac{1}{(S_1+S_2)^2}\left[S_1^2 \ln r_1 + S_2^2 \ln r_2 + 2S_1S_2 \ln d\right] \quad (23)$$

where S_1 represents the perimeter of one core wire of cable; S_2 represents the perimeter of another core wire; r_1 represents the radius of the S_1 core; r_2 represents the radius of the S_2 core; and d is the separation distance between the two parallel cores.

According to [16] and [17], the current distributions of the two halves of the equivalent asymmetrical dipole antenna along the x axis can be estimated as follows:

$$I_1(x) = \frac{4\pi V_{A1}}{\alpha_1 \eta} \times \frac{\sin k(l_1 - |x|) + M_1(l_1, x)/\alpha_1}{\cos(kl_1) + A_1(l_1)/\alpha_1}$$
$$0 < x < l_1$$
$$I_2(x) = \frac{4\pi V_{A2}}{\alpha_2 \eta} \times \frac{\sin k(l_2 - |x|) + M_2(l_2, x)/\alpha_2}{\cos(kl_2) + A_2(l_2)/\alpha_2}$$
$$-l_2 < x < 0 \quad (24)$$

where $\alpha_1 = 2ln(2l_1/b)$ and $\alpha_2 = 2ln(2l_2/a)$; η is the characteristic impedance of free space and equals 377 Ω; l_1 and l_2 are the arm lengths of the asymmetric antenna; a and b are arm radii of the asymmetric antenna; and k is the phase constant and equals $2\pi/\lambda$ (λ is the wavelength); $M(l, x)$ and $A(l)$ are auxiliary computational functions, their detailed expressions are given in the Appendix of [17] and they are not elaborated here for the sake of space; V_{A1} and V_{A2} are the equivalent driving voltage for the left arm and the right arm, respectively, and they can be calculated as follows:

$$V_{A1} = \Delta V_{C\text{total}} \frac{Z_1}{Z_1+Z_2}, \quad V_{A2} = \Delta V_{C\text{total}} \frac{Z_2}{Z_1+Z_2}. \quad (25)$$

The impedances Z_1 and Z_2 are given by the following:

$$Z_1 = \frac{\alpha_1 \eta}{4\pi} \times \frac{\alpha_1 \cos(kl_1) + A_1(l_1)}{\alpha_1 \sin(kl_1) + M_1(l_1, 0)}$$
$$Z_2 = \frac{\alpha_2 \eta}{4\pi} \times \frac{\alpha_2 \cos(kl_2) + A_2(l_2)}{\alpha_2 \sin(kl_2) + M_2(l_2, 0)}. \quad (26)$$

The far-field radiation of an asymmetric antenna in free space can be calculated according to the magnitude and the distribution of the current of (24). However, according to the EMC regulations, the electromagnetic radiated emission of a switched-mode power supply should be carried out in an open test field or a semi-anechoic chamber. The ground plane or the metal plane can reflect the incidental electromagnetic wave. This reflection effect should be considered in the radiation prediction process. Therefore, the mirror method is adopted to address the problem, which is presented in [15].

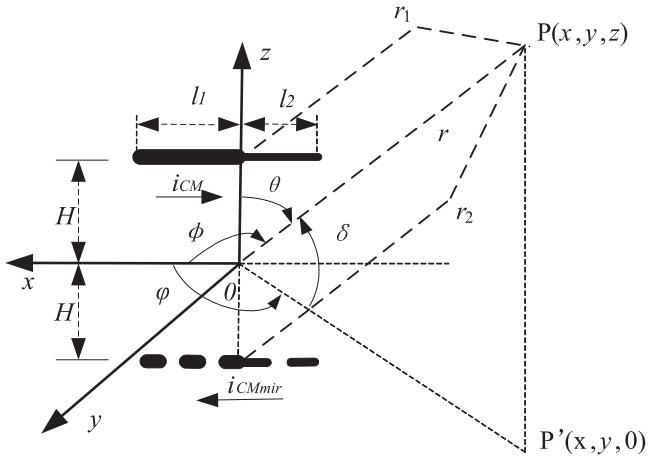

Fig. 7. CM radiation prediction model using the mirror method.

Fig. 7 shows the layout and coordinate system of the CM radiation prediction calculation, which includes the original asymmetric dipole antenna and the mirror dipole antenna (shown with thick dotted lines at the bottom of the figure). The *xoy* plane represents the infinite metal plane or ground plane, and H is the height measured from the equipment under test to the metal plane. The amplitude of the mirror CM current is the same as the original CM current; however, they flow in opposite directions. The far-field radiation strength is the sum of the radiations from both the original and the mirror CM currents. On the premise of a short dipole antenna, the formula of the estimated far-field strength at the observation point $P(x, y, z)$, for which the distance to the observation point is much longer than the total length of the cables, is listed in the following equation [15]:

$$E_{CM\phi} = -60\frac{e^{-jkr}}{r}\left[I_{l_1\max}\frac{\cos(kl_1\cos\phi) - \cos(kl_1) + j(\sin(kl_1\cos\phi) - \sin(kl_1)\cos\phi)}{\sin(\phi)}\right.$$
$$\left. + I_{l_2\max}\frac{\cos(kl_2\cos\phi) - \cos(kl_2) - j(\sin(kl_2\cos\phi) - \sin(kl_2)\cos\phi)}{\sin(\phi)}\right]\sin(kH\sin\delta) \quad (27)$$

where Φ is the angle between the axis of the antenna and the line connecting the observation point to the origin of the coordinate; δ is the angle between the line connecting the observation point to the origin of the coordinate and the *xoy* plane; φ is the angle between *xo*-axis to the line connecting $P'(x, y, 0)$ and the origin of the coordinate, $\varphi \approx \Phi$ when r is large enough; θ is the angle between the z-axis and the line connecting the observation point and the origin of the coordinate, and θ equals 90° minus δ; r is the distance between the observation point and the origin of the coordinate; and r_1 and r_2 are the distances between the center of the dipole antenna or mirror dipole antenna to the observation point P, respectively. In addition, $I_{l1\max}$ and $I_{l2\max}$ are the

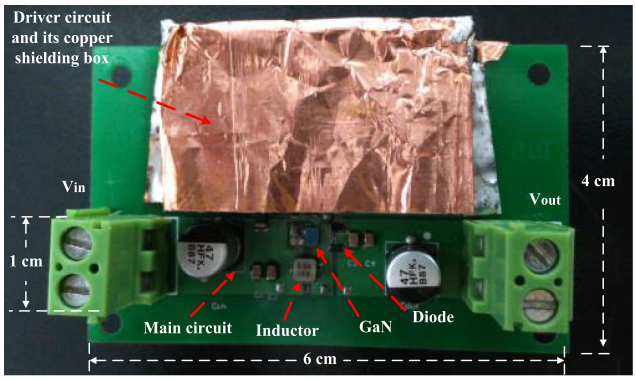

Fig. 8. VHF boost converter prototype with shielding.

maximum current on the left arm and the right arm of the dipole antenna, respectively, and their expressions under the thin wire case are given as follows [17]:

$$I_{l_1\max} = \frac{4\pi V_{A1}}{\alpha_1 \eta \left[\cos(kl_1) + A_1(l_1)/\alpha_1\right]}$$
$$I_{l_2\max} = \frac{4\pi V_{A2}}{\alpha_2 \eta \left[(\cos(kl_2) + A_2(l_2)/\alpha_2\right]}. \quad (28)$$

IV. Experimental and Simulation Verification

Combining the CM driving source with the radiation formulas, the far-field electromagnetic radiation of a nonisolated power converter with cables can be predicted. A low power VHF boost converter based on GaN is designed, and its CM radiated field strength is predicted and measured to verify the effectiveness of the proposed prediction method in this section. In addition, the radiation pattern characteristics are analyzed, and several restraint designs are also proposed and verified.

A. 30-MHz VHF Boost Converter Based on GaN and Its Waveforms

In order to concentrate on the radiation effect, a 30-MHz 4.5-W dc/dc boost converter based on GaN is designed and a prototype is constructed. Fig. 8 shows the top view of this prototype. Its size is 6 cm × 4 cm, and its main circuit is almost as the same as the circuit diagram shown in Fig. 4. The main design specifications are introduced here and summarized in Table I.

This VHF boost converter is controlled by a simple open-loop control mode to keep the switching waveforms stable. The driving signal of the GaN switch is generated by an XLMG1020 driver with a 30-MHz crystal oscillator. In order to make the DM radiation component as small as possible, without affecting the judgment of the CM radiation, two methods are adapted in advance. First, the driving signal circuit is shielded in a copper box, which is welded together with the negative pole of $V_{\rm in}$. Second, a 0.5 mm thin two-layer PCB board is used for the prototype, and the PCB traces of the main circuit are arranged in parallel, so that the area of the ac DM current loop is as small as possible. Actually, author's additional measurements show that the DM radiation from the converter itself is far less than the CM radiation in 30–300 MHz.

TABLE I
Specifications of the VHF Boost DC–DC Converter Prototype

Parameter & symbol	Value & unit
DC input voltage $V_{\rm in}$	6 V
DC output voltage $V_{\rm out}$	15 V
Output load	50 Ω
Switching frequency f_s	30 MHz
Inductor L	0.56 μH
Capacitor $C_{\rm in}$ $C_{\rm out}$	47 μF
Capacitor $C_{\rm in1}$ $C_{\rm in2}$ $C_{\rm out1}$ $C_{\rm out2}$	0.022 μF
Duty cycle ratio	40%
GaN semiconductor S	EPC2016C, 100 V, 18 A
Diode D	PMEG4020EPK, 40V, 2 A

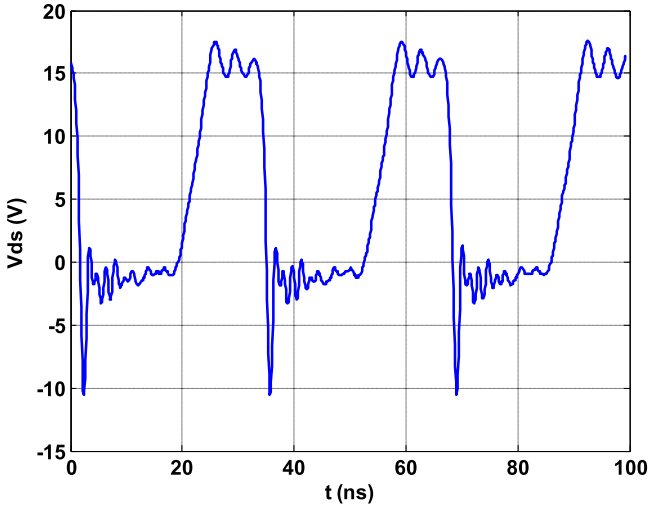

Fig. 9. Measured $V_{\rm ds}$ voltage waveform of the GaN switch.

Fig. 9 shows the $V_{\rm ds}$ waveform of the GaN switch under the rated load, which is measured with a wide bandwidth oscilloscope Tek DPO7254 and a 500-MHz bandwidth passive probe P6139A.

In the process of $\Delta V_{\rm Ctotal}$ waveform measurement, there are two technical problems that need attention. First, the ground clip of the passive probe should be kept as short as possible. In addition, the load effect of a passive probe needs to be considered and compensated to obtain the real $\Delta V_{\rm Ctotal}$ spectrum; i.e., $V_{oo\prime}$ voltage, as shown in Fig. 4.

According to Thevenin theorems, the equivalent source circuit model at the oo' port of the converter with cables can be shown [see Fig. 10(a)]. In this figure, $Z_{\rm internal}$ presents the equivalent internal impedance of the converter with cables; $Z_{\rm probe}$ presents the impedance of the passive probe; the measured voltage with probe is the $V_{oo'\rm mea}$ waveform in fact, and the real driving voltage $V_{oo'}$ can be obtained using (27) (Note: $V_{oo'}$ is the V_s when there is no probe.)

$$V_{oo'} = \left(1 + Z_{\rm internal}/Z_{\rm probe}\right) V_{oo'\rm mea}. \quad (29)$$

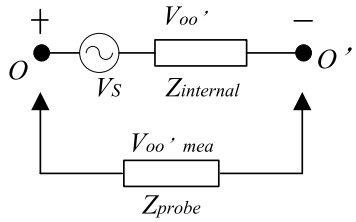

(a)

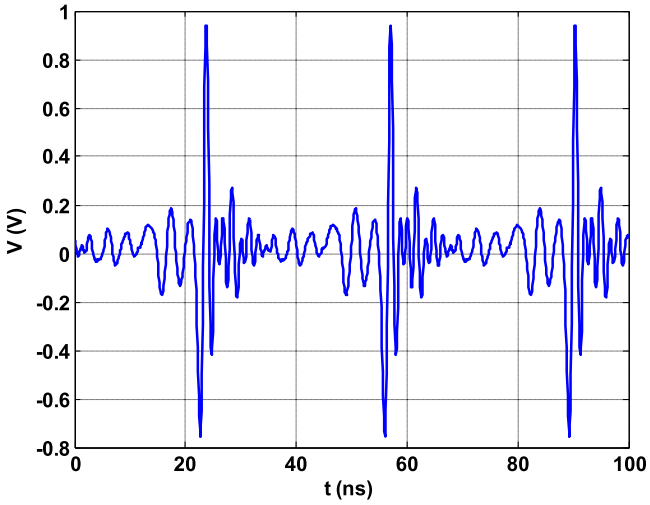

(b)

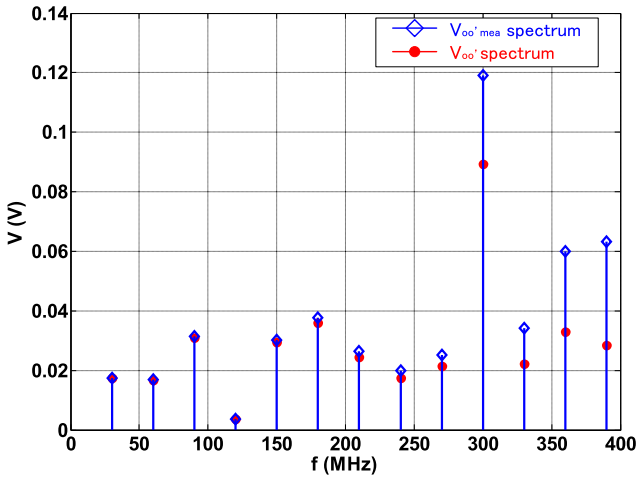

(c)

Fig. 10. Time domain waveform and spectrum of $\Delta V_{C\text{total}}$. (a) Measurement and compensation principle. (b) Measured waveform of $V_{oo'\text{mea}}$. (c) Spectrum of $\Delta V_{C\text{total}}$.

Fig. 10(b) shows the measured $V_{oo'\text{mea}}$ waveform of the VHF boost converter. This voltage waveform is obtained by measuring the voltage between O and O' point of the converter with Tek DPO7254 oscilloscope and P6139A probe. The spectrum of $V_{oo'\text{mea}}$ can be calculated via the fast Fourier transform algorithm and is shown with blue lines as 30-MHz interval in Fig. 10(c). After compensation process, the spectrum of driving voltage $V_{oo'}$ is shown with red points in Fig. 10(c).

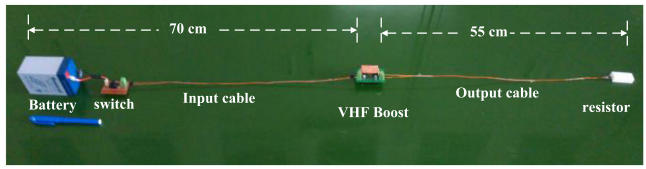

Fig. 11. Test layout of the VHF boost converter with power cables.

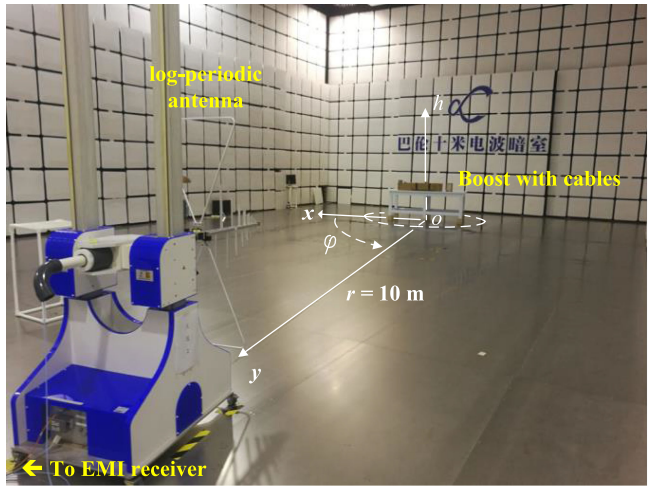

Fig. 12. Far-field measurement setup in a 10 m semi-anechoic chamber.

The impedance of Z_{internal} and Z_{probe} are measured using Agilent 4396b impedance analyzer. It is noteworthy that the highest amplitude occurs at the 300 MHz frequency; careful observations reveal this is the ring frequency when the GaN switch is turned OFF.

B. CM Radiation Prediction and Verification

The actual VHF boost power converter with power cables is shown in Fig. 11. The effective length of the input cable is 70 cm and the length of output cable is 55 cm. Both the input and output cables are made of two enameled copper wires with a diameter of 1 mm, and these two cables are aligned from the left to the right in the test layout. The distance between centers of enameled wires arranged in parallel is 1 mm, and the circular conductor radius r_e of the equivalent asymmetric dipole antenna is calculated to be 0.707 mm, according to (23).

According to the EMC radiation standard CISPR 22 of general electronic equipment, the radiation of the VHF boost converter with cables is tested in a 10-m semi-anechoic chamber. Fig. 12 shows the electric field measurement setup. The height of the Boost converter with cables is 1 m from the metal ground plane. The distance from the receiver antenna to the converter is 10 m. In the test, the log-periodic receiver antenna changes the received electric field signal into a voltage signal and sends it to an electromagnetic interference (EMI) receiver (or a spectrum analyzer) through a coaxial cable. The EMI receiver gets the measured electric field strength after the antenna factor conversion.

The frequency domain far-field electric strength and distribution can be calculated by the spectrum of the equivalent

CM driving voltage source $V_{C\text{total}}$ and the asymmetric dipole antenna algorithms introduced in Section III. Fig. 13 shows the predicted and measured field strengths at several typical observation locations, i.e., the receiver antenna positions. The cylindrical coordinates of the observation locations are: (10 m, 90°, 1 m), (10 m, 45°, 1 m), and (10 m, 90°, 4 m), respectively. As the horizontal component of the electric field of a horizontal layout wire radiator is generally larger than the vertical component, only the predicted and measured values of the horizontal electric field are shown in Fig. 13.

From Fig. 13, the predicted and measured electric strengths are generally consistent. At most harmonic frequencies, the prediction error is approximately 3–6 dB, with a few exceptions at frequency points below 300 MHz. Here, feature selective validation method is further used to quantify and evaluate the consistency between predicted data and measured data [18], [19]. The average GRADE value and SPREAD value of the data of Fig. 13(a)–(c) is (2.9, 2.5), (4.2, 3.5), and (2.4, 2), respectively. It means the predicted data are with good or very good consistency for Fig. 13(a) and (c). The predicted data of Fig. 13(b) have a fair consistency. In fact, one of the reasons for the lower evaluation value of Fig. 13(b) data is that the measured value at 30 MHz is background noise, not the real radiation value. Generally speaking, the above measurement results confirm the feasibility and validity of the prediction method.

In the predicted results above, there also are some clear deviations that occur at some frequency points in addition to the 30 MHz. This phenomenon may be due to the ±4 dB error tolerances range of the radiation test site, in addition to simplifying assumptions made in the model (e.g., neglect to consider the volume of battery and inductor, influence of DM current radiation, coupling effect of PCB traces, etc.).

C. CM Radiation Characteristics Analysis

The magnitude of the far-field electric strength depends naturally on both the magnitude of the CM driving source and the efficiency of the radiator. For this asymmetric dipole radiator, the maximum radiation efficiency should occur near 120, 240 MHz according to the half-wave antenna principle. However, the 4th and 8th even-frequency harmonic amplitudes of the $V_{oo'}$ voltage are lower [from Fig. 10(b)], resulting in a lower radiation electric strength around 120 and 240 MHz. The third odd-frequency harmonics of $V_{oo'}$ has a higher amplitude, and ultimately leads to a larger electric strength at 90 MHz. The magnitude of the 10th harmonic of $V_{oo'}$ is the highest, plus its radiation efficiency is not low: it produces the strongest RE around 300 MHz.

The electromagnetic radiation also has obvious directionality. Fig. 14 shows the three-dimensional radiation pattern of the boost asymmetric antenna system at typical frequencies of 90 and 300 MHz, which are simulated and drawn by Ansoft HFSS software. The red color means a stronger electric strength and the light color represents a lower electric strength. At 90 MHz, the radiator length is shorter than the wavelength, and the radiation pattern of this boost converter with cables is similar to that of traditional half-wave dipole: only a main lobe exists and the

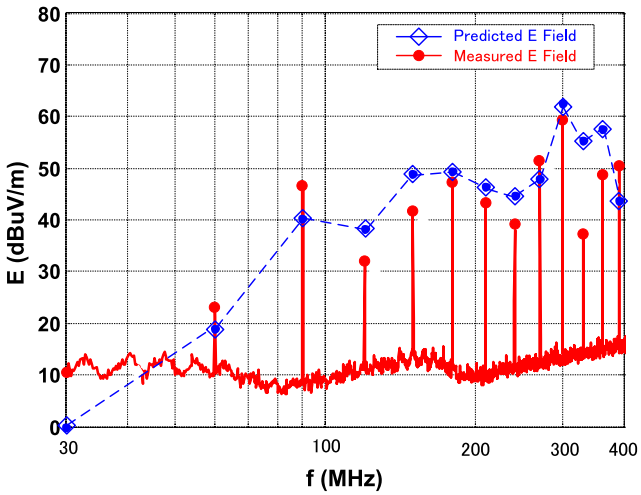

(a)

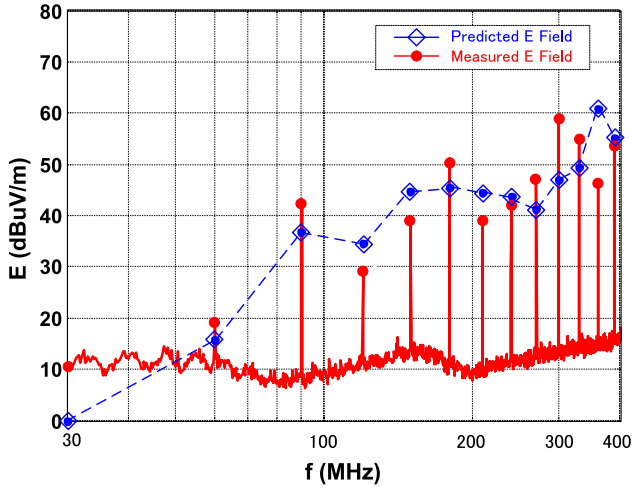

(b)

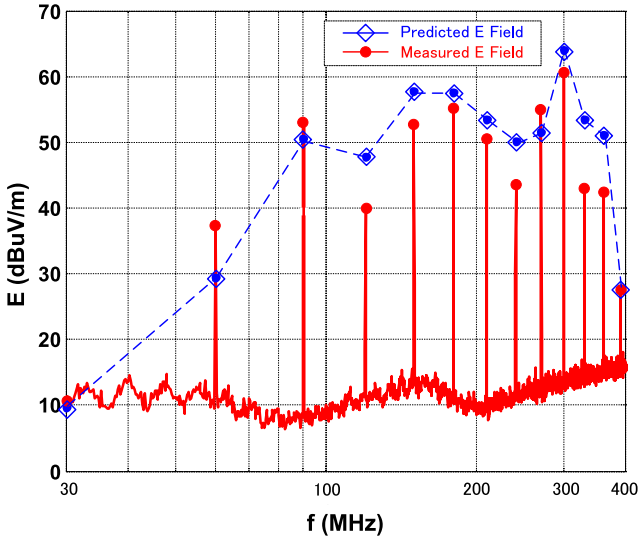

(c)

Fig. 13. Comparison of the predicted and measured electric strength. (a) $r_c = 10$ m, $\varphi = 90°$, $h = 1$ m. (b) $r_c = 10$ m, $\varphi = 45°$, $h = 1$ m. (c) $r_c = 10$ m, $\varphi = 90°$, and $h = 4$ m. (Note: r_c is the distance between the projection of the observation point on the *xoy* plane and the origin.)

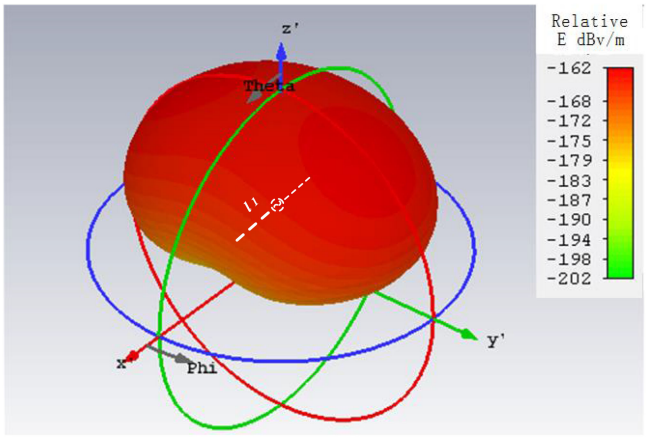

(a)

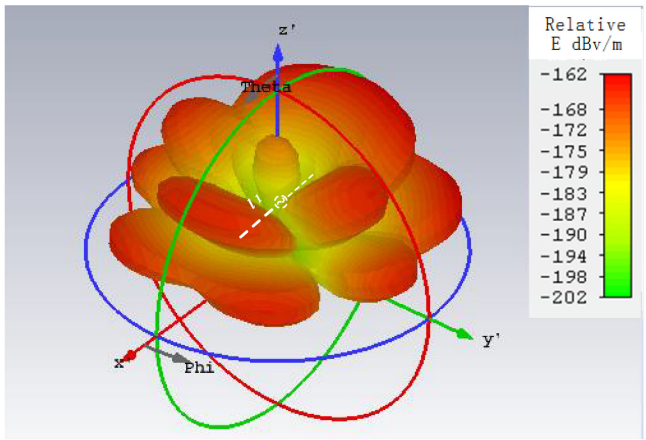

(b)

Fig. 14. CM radiation pattern of the boost converter with cables. (a) 90 MHz. (b) 300 MHz.

y-axis direction is the maximum radiation direction. It is also easy to see that the electric strength below the cable's height decreases greatly, due to the influence of ground reflection. At 300 MHz, the radiation pattern changes significantly, as many lobes appear. This also indicates that it is more challenging to predict radiation accurately at higher frequencies.

D. Radiation Reduction Designs

Both reducing the amplitude of the CM noise source and the radiating current of the emitter are effective methods to suppress CM radiation according to the radiation mechanism derived in this article. Two radiation suppression methods are introduced and tested below.

The equivalent CM driving voltage, $\Delta V_{\mathrm{Ctotal}}$, can be reduced by inserting DM filters at the input and output ports. According to (22), this decreases both the V_{in} and V_{out} terms. Fig. 15(a) shows the actual *LC* type DM filters and their insertion position. The surface mounted device (SMD) DM inductor model is R56, and its inductance is 0.56 μH. The SMD C_x capacitors are nonpolar 0.22 μF. Fig. 15(b) shows the measured electric strength at the same observation position with/without DM filters. There is a

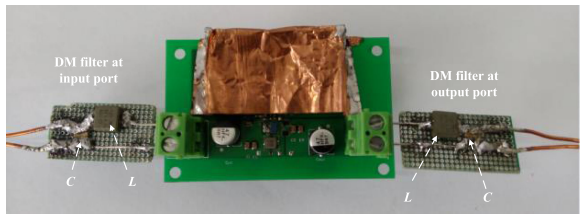

(a)

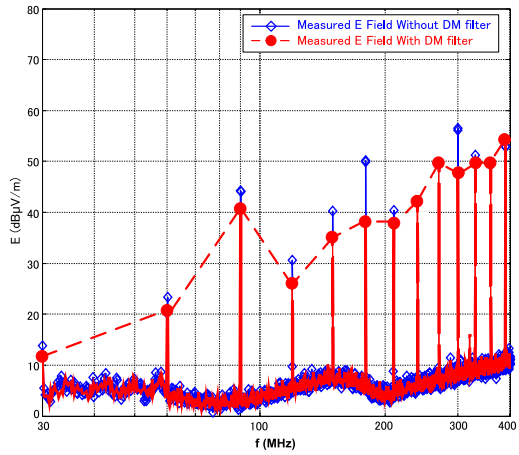

(b)

Fig. 15. DM filter design at the input/output port. (a) Actual DM filters. (b) Measured electric strength at ($r_c = 10$ m, $\varphi = 90°$, and $h = 1$ m) w/wo DM filters.

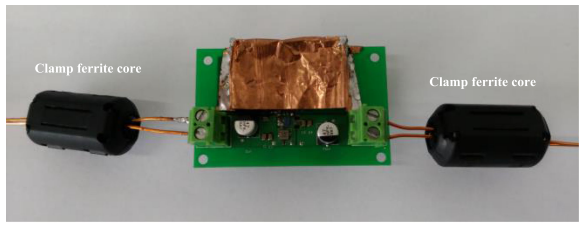

(a)

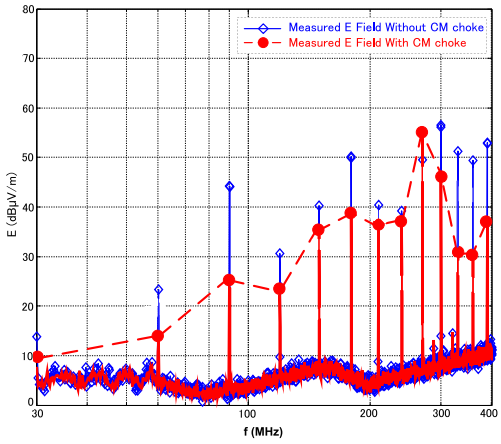

(b)

Fig. 16. CM chokes inserted at the input/output port. (a) Actual clamp ferrite cores. (b) Measured electric strength at ($r_c = 10$ m, $\varphi = 90°$, and $h = 1$ m) w/wo clamp ferrite cores.

2–7 dB magnitude decrease below 200 MHz, and these results show the effectiveness of the DM filtering proposed.

A high-frequency CM choke, which is typically made of a nickel-zinc core with low permeability, can retain larger inductance and resistance values even in the radiated frequency band. When a choke is connected to the cables near the input or output port, it can naturally change two characteristics. First, the resonant frequencies of the cable radiation antenna are modified. Second, the radiation damping is increased, which attenuates the amplitude of CM current [13], [20]. This article inserts high-frequency clamp ferrite cores at the input and output cables. Fig. 16(a) shows the actual clamp ferrite cores and their insertion positions. The clamp ferrite core model is UF-90B. Fig. 16(b) shows the measured electric strengths at the same observation position with/without clamp ferrite cores. Clearly, there is 4–18 dB magnitude decrease below 240 MHz, and the results also prove the effectiveness of the traditional high-frequency CM choke method.

V. Conclusion

In this article, the CM radiation formation mechanism and prediction algorithms of a nonisolated dc/dc converter with cables are analyzed, deduced, and verified in depth. The experimental results of a VHF boost power converter show that the methods achieve good results below 300 MHz. Based on the generalized CM potential definition and the theoretical analysis, it is found that the equivalent CM driving voltage source of the converter is composed of the input/output voltage noises and the PCB ground voltage. The far-field electric strength and its spatial distribution of the asymmetric wire antenna composed of input/output cables are also clearly influenced by frequency and the reflection of the metal ground plane. The research methods and results of this article provide a useful theoretical reference for radiation analysis, prediction, and improvement of other types of power electronic equipment.

On the basis of this article, there is still more work to be done on the far-field radiation prediction method and the radiation suppression design for a power converter. The cause of the prediction error requires an in-depth analysis, and a further improved CM radiation prediction model is planned for development, which includes the volume influence of the battery and loads. In addition, a reasonable design of radiation suppression is a future goal of this study. Combined with DM radiation, the comprehensive prediction of RE in a wider frequency band (30 MHz–1 GHz) is also a field worthy of in-depth study for the new generation of power converters based on wide band-gap semiconductor switches.

References

[1] G. Antonini, S. Cristina, and A. Orlandi, "EMC characterization of SMPS devices: Circuit and radiated emissions model," *IEEE Trans. Electromagn. Compat.*, vol. 38, no. 3, pp. 300–309, Aug. 1996.

[2] V. Tarateeraseth, "Educational laboratory experiments on EMC in power electronics," *IEEE Electromagn. Compat. Mag.*, vol. 3, no. 3, pp. 55–60, Aug. 2014.

[3] E. A. Jones, F. F. Wang, and D. Costinett, "Review of commercial GaN power devices and GaN-based converter design challenges," *IEEE J. Emerg. Sel. Topics Power Electron.*, vol. 4, no. 3, pp. 707–719, Sep. 2016.

[4] D. Aggeler, F. Canales, J. Biela, and J. W. Kolar, "Dv/Dt control methods for the SiC JFET/Si MOSFET cascade," *IEEE Trans. Power Electron.*, vol. 28, no. 8, pp. 4074–4082, Aug. 2013.

[5] C. R. Paul, "A comparison of the contributions of common-mode and differential-mode currents in radiated emissions," *IEEE Trans. Electromagn. Compat.*, vol. 31, no. 2, pp. 189–193, May 1989.

[6] X. Tong, D. W. P. Thomas, A. Nothofer, P. Sewell, and C. Christopoulos, "Modeling electromagnetic emissions from printed circuit boards in closed environments using equivalent dipoles," *IEEE Trans. Electromag. Compat.*, vol. 52, no. 2, pp. 462–470, Mar. 2010.

[7] C. Su and T. H. Hubing, "Calculating radiated emissions due to I/O line coupling on printed circuit boards using the imbalance difference method," *IEEE Trans. Electromagn. Compat.*, vol. 54, no. 1, pp. 212–217, Feb. 2012.

[8] H. Chen, T. Wang, L. Feng, and G. Chen, "Determining far-field EMI from near-field coupling of a power converter," *I EEE Trans. Power Electron.*, vol. 29, no. 10, pp. 5257–5264, Oct. 2014.

[9] H. Zhang, Y. Zhang, and S. Wang, "Radiated EMI modeling of the non-isolated DC-DC power converters with attached cables," in *Proc. IEEE Energy Convers. Congr. Expo.*, 2018, pp. 4203–4209.

[10] T. Watanabe, O. Wada, T. Miyashita, and R. Koga, "Common-mode current generation caused by difference of unbalance of transmission lines on a printed circuit board with narrow ground pattern," *IEICE Trans. Commun.*, vol. E83-B, no. 3, pp. 593–599, Mar. 2000.

[11] D. M. Hockanson, J. L. Drewniak, T. H. Hubing, T. P. Van Doren, F. Sha, and M. J. Wilhelm, "Investigation of fundamental EMI source mechanisms driving common-mode radiation from printed circuit boards with attached cables," *IEEE Trans. Electromagn. Compat.*, vol. 38, no. 4, pp. 557–566, Nov. 1996.

[12] J. He, Y. Gao, and K. Ji, "Model and simulation on common mode radiation of a flyback power supply," in *Proc. Asia-Pac.Symp. Electromagn. Compat.*, May 2012, pp. 117–120.

[13] Y. Zhang, S. Wang, and Y. Chu, "Investigation of radiated electromagnetic interference for an isolated high frequency DC-DC power converter with power cables," *I EEE Trans. Power Electron.*, vol. 34, no. 10, pp. 9632–9643, Oct. 2019.

[14] C. R. Paul, *Analysis of Multiconductor Transmission Lines*, 1st ed. Hoboken, NJ, USA: Wiley, 1994.

[15] C.A. Balanis, *Antenna Theory: Analysis and Design*, 3rd ed. Hoboken, NJ, USA: Wiley, 2016.

[16] N. Zhang, J. Kim, and S. Ryu, "Prediction of common-mode radiated emission of PCB with an attached cable using imbalance difference model," *IEICE Trans. Commun.*, vol. E98-B, no. 4, pp. 638–645, Apr. 2015.

[17] R. King and C. Harrison, "The distribution of current along a symmetrical center-driven antenna," *Proc. IRE*, vol. 31, no. 10, pp. 548–567, Oct. 1943.

[18] Standard for Validation of Computational Electromagnetics Computer Modeling and Simulation, IEEE Std. 1597.1-2008-IEEE, 2008.

[19] A. P. Duffy, A. J. M. Martin, A. Orlandi, G. Antonini, T. M. Benson, and M. S. Woolfson, "Feature selective validation (FSV) for validation of computational electromagnetics (CEM). Part 1—The FSV method," *IEEE Trans. E lectromagn. C ompat.*, vol. 48, no. 3, pp. 460–467, Aug. 2006.

[20] C. Hsiao, C. Tsai, C. Chiu, and T. Wu, "Radiation suppression for cable-attached packages utilizing a compact embedded common-mode filter," *IEEE Trans. Compon., Packag. Manuf. Technol.*, vol. 2 no. 10, pp. 1696–1703. Oct. 2012.

Junping He (Member, IEEE) received the bachelor's and master's degrees from the the Northern Jiaotong University, Beijing, China, in 1993 and 1999, respectively, and the Ph.D. degree from Tsinghua University, Beijing, China, in 2003, all in electrical engineering.

He engaged in near field coupling effect research as a Postdoctoral of Tsinghua University and Delta Power Electronics Center (DPEC), Shanghai, China, from 2003 to 2005. In 2005, he joined the Harbin Institute of Technology (Shenzhen), Shenzhen, China, where he is currently an Associate Professor. His research interests include electromagnetic compatibility analysis and design in power electronics, and renewable energy power generation.

Zichao Guo (Student Member IEEE) received the bachelor's degree in electrical engineering from the Hebei University of Techonlogy, Tianjing, China, in 2016, and the master's degree in electrical engineering from the Harbin Institute of Technology (Shenzhen), Shenzhen, China, in 2019.

His main research field is electromagnetic compatibility of power electronics. He is currently an Engineer with Hikvision Company, Hangzhou, China, where he is mainly engaged in the development of automotive electronics.

Xin Li received the bachelor's degree in electrical engineering from Yanshan University, Qinhuangdao, China, in 2015, and the master's degree from the Harbin Institute of Technology (Shenzhen), Shenzhen, China, in 2018.

She is currently an Engineer with Huawei Company, Beijing, China, where she is mainly engaged in the electromagnetic design of electronics. Her research interests include electromagnetic compatibility, power electronics and its control.